

---

# Differentially Private Geodesic and Linear Regression

---

**Aditya Kulkarni**  
 Department of Physics  
 University of Massachusetts Amherst  
 Amherst, MA 01003  
 abkulkarni@umass.edu

**Carlos Soto**  
 Department of Mathematics and Statistics  
 University of Massachusetts Amherst  
 Amherst, MA 01003  
 carlossoto@umass.edu

## Abstract

In statistical applications it has become increasingly common to encounter data structures that live on non-linear spaces such as manifolds. Classical linear regression, one of the most fundamental methodologies of statistical learning, captures the relationship between an independent variable and a response variable which both are assumed to live in Euclidean space. Thus, geodesic regression emerged as an extension where the response variable lives on a Riemannian manifold. The parameters of geodesic regression, as with linear regression, capture the relationship of sensitive data and hence one should consider the privacy protection practices of said parameters. We consider releasing Differentially Private (DP) parameters of geodesic regression via the K-Norm Gradient (KNG) mechanism for Riemannian manifolds. We derive theoretical bounds for the sensitivity of the parameters showing they are tied to their respective Jacobi fields and hence the curvature of the space. This corroborates recent findings of differential privacy for the Fréchet mean. We demonstrate the efficacy of our methodology on the sphere,  $\mathbb{S}^2 \subset \mathbb{R}^3$  and, since it is general to Riemannian manifolds, the manifold of Euclidean space which simplifies geodesic regression to a case of linear regression. Our methodology is general to any Riemannian manifold and thus it is suitable for data in domains such as medical imaging and computer vision.

## 1 Introduction and Motivation

One of the most foundational tools in statistical analyses is linear regression. In its simplest form, linear regression learns a linear relationship between an independent variable, the predictor, and a dependent variable, the response. Typically, these variables are both assumed to lie in a flat, Euclidean space. However, in modern statistical practices, it is common to encounter data that inherently live in curved non-Euclidean spaces such as spherical data (e.g. directional wind data, spatial data, square-root discrete distributions) [Fisher et al., 1993, Jeong et al., 2017], symmetric positive definite matrices (e.g. covariance matrices, brain tensors) Fletcher and Joshi [2004]. For this reason, there have been many different extensions of regression to non-linear spaces; Faraway [2014] considered regression on metric spaces only requiring pairwise distances between the observations, Wasserstein Regression Chen et al. [2023] captures the relationship between univariate distributions as predictors and either distributions or scalars as the response, Fréchet Regression Petersen and Müller [2019] captures the relationship between Euclidean predictors and responses that lie in a metric space, and Geodesic Regression Fletcher [2011] captures the relationship between Euclidean predictors and response variables that lie on a Riemannian manifold, for instance.

Whatever space the data may live, the learned relationship between variables relies on data captured from individuals; these individuals may be concerned with safeguarding their sensitive data. To protect one’s data, differential privacy [Dwork et al., 2006, DP] has emerged as a leading standard for data sanitisation. Perhaps surprisingly, differential privacy for a methodology as fundamental as

linear regression is not so straightforward. A common approach for private linear regression involves sanitizing the matrix  $A^T A$  which was explored by Sheffet [2019], Dwork et al. [2014], although the latter considered this in the case of private PCA, where  $A$  is the matrix of data with rows being observations and columns being features. Wang [2018], Sheffet [2017], and Alabi et al. [2020] survey the landscape of techniques as well as propose their own algorithms, so all this is to say that the fundamental and seemingly simple task is not trivial.

Recently, there has been an emergence of extensions of differential privacy techniques into Riemannian manifolds; Reimherr et al. [2021] considered privately estimating the Fréchet mean on Riemannian manifolds and, in the process thereof, extended the Laplace mechanism. They note that the sensitivity of the Fréchet mean is tied to the curvature of space and inflated for positively curved manifolds. They further note that sanitising on the manifold incurs less noise than sanitising in an ambient space under the same privacy budget. Following this work, mechanism design for manifolds has been developed such as the  $k$  norm gradient mechanism for manifolds Soto et al. [2022], DP Riemannian optimization Han et al. [2024a,b], and extensions of DP definitions such as Gaussian DP for manifolds Jiang et al. [2023],

In this paper, we consider the problem of privately estimating the parameters of geodesic regression Fletcher [2011], regression with a Euclidean predictor, and a response variable on a Riemannian manifold. Geodesic regression is parametrised by a footpoint, an initial value on the manifold, and a shooting vector, the average direction of data; our method sanitizes the parameters separately with the Riemannian manifold extension of K-Norm Gradient mechanism Reimherr and Awan [2019], Soto et al. [2022]. We show that the sensitivity of each parameter is tied to their respective Jacobi field equations and hence the curvature of the manifold. We demonstrate our methodology on the sphere with simulated data. Our methodology, however, is general to any Riemannian manifold and simply requires an understanding of the Jacobi fields which are specific to the manifold of interest. For instance, this could be adapted to Kendall shape space Kendall [1984] to show the evolution of an average shape throughout time in a private manner.

Building on our differentially private geodesic regression model, we consider linear regression as a special case by restricting our Riemannian manifold to four-dimensional Euclidean space,  $\mathbb{R}^4$ . This allows us to implement differentially private linear regression within the same framework. We evaluate our model’s performance against two existing state-of-the-art private linear regression tools: IBM Diffpriv [Holohan et al., 2019] and OPACUS [Yousefpoor et al., 2022].

## 2 Background and Notation

### 2.1 Riemannian Manifolds

In the following, we summarize the necessary tools of differential geometry for handling Riemannian manifolds. Some additional details can be found in C and we refer to classical texts such as Do Carmo [1992] and Nakahara [2018] for a more thorough introduction.

A manifold  $\mathcal{M}$  is a topological space that is locally equivalent to Euclidean space  $\mathbb{R}^n$ . A manifold can be further endowed with a metric giving it additional structure such as the ability to measure angles and lengths. This is a natural generalization of the inner product between vectors in  $\mathbb{R}^n$  to an arbitrary manifold. A Riemannian metric  $g : T_p\mathcal{M} \mapsto \mathbb{R}$  is a  $(0, 2)$  tensor field on  $\mathcal{M}$  that is symmetric  $g_p(U, V) = g_p(V, U)$  and positive definite  $g_p(U, U) \geq 0$  where  $U, V$  lie on the tangent space of  $\mathcal{M}$  at  $p$  denoted by  $T_p\mathcal{M}$ . A smooth manifold that admits a Riemannian metric is called a Riemannian manifold.

We can define an exponential map at point  $p \in \mathcal{M}$  as  $\text{Exp}(p, v) := \gamma_v(1)$  where  $\gamma : [0, 1] \rightarrow \mathcal{M}$  is a geodesic. The exponential map, maps a vector  $v \in T_p\mathcal{M}$  to  $\gamma(1) \in \mathcal{M}$ . Similarly, we can define the inverse of the exponential map, the log map,  $\text{Log}_p : P \rightarrow T_p\mathcal{M}$  where  $P \subset \mathcal{M}$  is the largest normal neighborhood of  $p$ . We use parallel transport to compare and combine vectors on different tangent spaces of a manifold. Parallel transport provides a way to move tangent vectors along a curve while preserving their length from one tangent space to another. Given a smooth curve  $\gamma(t)$  starting at point  $p$ , parallel transport ensures that the vector  $v(t)$ ,  $v \in T_p\mathcal{M}$ , remains ‘straight’ relative to the manifold’s curvature as it moves along the curve  $\gamma(t)$  by satisfying  $\nabla_{\dot{\gamma}(t)} v(t) = 0$ . We denote  $\Gamma_p^q v$  as the parallel transport of vector  $v \in T_p\mathcal{M}$  to the tangent space  $T_q\mathcal{M}$ . Since parallel transport moves tangent vectors along smooth paths in a parallel sense, it preserves the Riemannian metric

and hence angles between vectors. That is, for a smooth curve  $\gamma : [0, 1] \rightarrow \mathcal{M}$  and tangent vectors  $v_1, v_2 \in T_{\gamma(0)}\mathcal{M}$  we have that  $\langle v_1, v_2 \rangle_{\gamma(0)} = \left\langle \Gamma_{\gamma(0)}^{\gamma(1)} v_1, \Gamma_{\gamma(0)}^{\gamma(1)} v_2 \right\rangle_{\gamma(1)}$ .

Geodesics on a manifold are affected by the curvature of the manifold. Roughly, positive curvature causes geodesics to converge and negative curvature causes geodesics to diverge. Jacobi equations are a way of quantifying this dependence of curvature on the geodesic. A vector field satisfying the Jacobi equation is called a Jacobi field. For a geodesic  $\gamma$  and a vector field  $J$  along  $\gamma$ , the Jacobi equation is defined as,

$$\frac{D^2}{dt^2} J(t) + R \left( J(t), \frac{d}{dt} \gamma \right) \frac{d}{dt} \gamma = 0, \quad (1)$$

where  $R$  is the Riemannian curvature tensor, see C.2. An important result of Riemannian geometry that will be useful later is the Rauch theorem, which states:

**Theorem 2.1** (Rauch Comparison Theorem). *For two Riemannian manifolds  $\mathcal{M}, \tilde{\mathcal{M}}$  with curvatures  $K(\gamma), \tilde{K}(\tilde{\gamma})$  and unit speed geodesics  $\gamma : [0, \beta] \rightarrow \mathcal{M}$  and  $\tilde{\gamma} : [0, \beta] \rightarrow \tilde{\mathcal{M}}$  and  $J, \tilde{J}$  be the Jacobi fields along  $\gamma, \tilde{\gamma}$ , respectively. If  $K(\gamma) \leq \tilde{K}(\tilde{\gamma})$  then,*

$$\|\tilde{J}\| \leq \|J\|. \quad (2)$$

Intuitively, this states that for large curvature geodesics tend to converge, while for small (or negative) curvature geodesics tend to spread. As curvature increases, lengths shorten. We use this to bound the norm of the Jacobi field on a manifold with curvature bounded from above.

## 2.2 Geodesic and Linear Regression

Geodesic regression provides a framework for modeling the relationship between a real-valued independent variable and a manifold-valued dependent variable, leveraging the intrinsic geometry of Riemannian manifolds. Unlike traditional linear regression, geodesic regression generalizes the concept to non-linear spaces, representing relationships as geodesic curves on the manifold. Fletcher [2011] formulated the least-squares estimation of geodesic regression by minimizing the sum of squared geodesic distances between data points and the estimated prediction geodesic. Consider a dataset  $D = \{(x_i, y_i)\}$  where  $(x_i, y_i) \in \mathbb{R} \times \mathcal{M}$ , for  $i = 1, \dots, n$ . Here  $x_i$  lie on the real line and can be scaled to be between  $(0, 1)$  and  $y_i$  lie on a Riemannian manifold  $\mathcal{M}$ . To estimate the regression parameters,  $(p, v) \in T\mathcal{M}$  we need to minimise the least squared energy given by:

$$E(p, v) = \frac{1}{2n} \sum_{i=1}^n d(\text{Exp}(p, x_i v), y_i)^2, \quad (3)$$

$$(\hat{p}, \hat{v}) = \underset{(p, v)}{\text{argmin}} E(p, v). \quad (4)$$

Here,  $d(\cdot, \cdot)$  is the geodesic distance on the manifold, so the energy is the sum of square distances from the predicted value,  $\text{Exp}(p, x_i v)$ , and the observed value,  $y_i$ . This framework enables parametrisation through an initial point, or footpoint, and velocity, or shooting vector. This is analogous to an intercept and slope in linear regression. To solve the ordinary least squared minimization problem Fletcher [2011] derived a gradient descent algorithm for the sum-of-squares energy given in Eqn. 3. The gradient of the energy with respect to the footpoint ( $p$ ) and the shooting vector ( $v$ ) are given by,

$$\nabla_p E = - \sum_{i=1}^n d_p \text{Exp}(p, x_i v)^\dagger \epsilon_i, \quad (5)$$

$$\nabla_v E = - \sum_{i=1}^n x_i d_v \text{Exp}(p, x_i v)^\dagger \epsilon_i, \quad (6)$$

respectively, where the errors are defined as:  $\epsilon_i = \text{Log}(\text{Exp}(p, x_i v), y_i)$ . Further, for existence and uniqueness of the optimal solutions, only geodesics “close” to the data are considered where a geodesic  $\gamma$  is defined as  $\tau$ -close if  $d(\gamma(x_i), y_i) \leq \tau$  for all  $i$ ,  $\tau > 0$ , and  $\gamma$  does not pass through the cut locus of the manifold.

As opposed to linear regression, where the errors are scalar values, here the errors are vectors in the tangent spaces of the predicted values,  $T_{\text{Exp}(p, x_i v)}\mathcal{M}$ . The derivative of the exponential map with respect to the footpoint  $p$  can be calculated by varying  $p$  along the geodesic

$\eta(s) = \text{Exp}(p, s u_1)$ , where  $u_1 \in T_p \mathcal{M}$ . This will result in the variation of the geodesic given by  $c_1(s, t) = \text{Exp}(\text{Exp}(p, s u_1), t v(s))$ . Similarly, the derivative of the exponential map with respect to the shooting vector  $v$  is found by a varying  $v$  resulting in the variation of geodesic  $c_2(s, t) = \text{Exp}(p, s u_2 + t v)$ , where  $u_2 \in T_p \mathcal{M}$ . This gives the derivatives of the exponential map as:

$$d_p \text{Exp}(p, v) \cdot u_1 = J_1(1), \quad (7)$$

$$d_v \text{Exp}(p, v) \cdot u_2 = J_2(1), \quad (8)$$

where  $J_i(t)$  are Jacobi fields along the geodesic  $\gamma(t) = \text{Exp}(p, t v)$ .

A special case of Geodesic Regression is when one takes the Riemannian manifold as the Euclidean space,  $\mathcal{M} = \mathbb{R}^n$ , leading to a case of Multiple Linear Regression. The linear model for  $Y \in \mathbb{R}^n$  and  $X \in \mathbb{R}$  is given by;  $Y = \alpha + X \beta + \epsilon$ . Here  $\alpha, \beta$  are the intercept and the slope parameters respectively and  $\epsilon$  is the error. In terms of the Geodesic Regression parameters,  $\alpha$  is the footpoint of the line, and  $\beta$  is the (velocity) shooting vector. The least-squares estimates for the intercept and the slope are given by:

$$(\hat{\alpha}, \hat{\beta}) = \underset{(\alpha, \beta)}{\text{argmin}} \sum_{i=1}^N \|y_i - \alpha - \beta x_i\|^2. \quad (9)$$

### 2.3 Differential Privacy

In the modern era of data collection, the protection of privacy of one's data has become increasingly prevalent. There is no one consensus on what one means by *privacy*. However, *differential privacy* Dwork et al. [2006] has recently become the defacto definition. Since its initial definition there have been many extensions and alternate definitions such as concentrated DP [Dwork and Rothblum, 2016], zero-concentrated DP (zCDP) [Bun and Steinke, 2016], Rényi differential privacy [Mironov, 2017], and Gaussian differential privacy ( $\mu$ -GDP) [Dong et al., 2022], for instance. Even though there are different forms of differential privacy, all definitions rely on the idea of *adjacent* datasets.

Let  $D = \{(x_1, y_1), \dots, (x_n, y_n)\} \subset (\mathbb{R} \times \mathcal{M})$  denote a dataset of size  $n$ . An adjacent dataset  $D'$  differs from  $D$  in exactly one record or observation which we can take, without loss of generality, to be the last i.e.  $D' = \{(x_1, y_1), \dots, (x'_n, y'_n)\}$ . Adjacent datasets are denoted as  $D \sim D'$ .

**Definition 2.2.** A randomised mechanism  $f(x; D)$  is said to satisfy *pure differential privacy* if

$$P(f(x; D) \in A) \leq \exp(\epsilon) P(f(x; D') \in A),$$

for given privacy budget  $\epsilon > 0$ ,  $D \sim D'$ , and  $A$  is any measurable set in  $\mathcal{M}$ .

Roughly speaking, for small  $\epsilon$ , a mechanism that satisfies pure differential privacy is approximately equally likely to observe a realization from the random mechanism over all adjacent datasets. This definition of privacy is attractive as it ensures noise calibration relative to an individual's effect on the mechanism relative to the entire dataset. Differential privacy is well defined over Riemannian manifolds via the Riemannian measure [Reimherr et al., 2021] as it is well defined over measurable spaces [Wasserman and Zhou, 2010]. An attractive property of this definition is the composition of mechanisms. Given two mechanisms  $f_1, f_2$  with privacy budgets  $\epsilon_1, \epsilon_2$ , respectively, the total privacy budget is  $\epsilon_1 + \epsilon_2$ . Note these  $\epsilon$  are privacy budgets and not the errors from 2.2.

We wish to release private versions of the parameters  $(p, v)$ , the footpoint, and the shooting vector of geodesic regression, respectively. Generally speaking, these parameters are not available in closed form but rather are optimizers of an energy function. The exponential mechanism [McSherry and Talwar, 2007] is a randomized mechanism that releases values nearly optimizing an energy function. Generally, it takes the form

$$f(z; D) \propto \exp\{-\sigma^{-1} E(z; D)\},$$

where  $\sigma$  is a spread parameter which determines the noise scale,  $E(z; D)$  is an energy function to be minimized, and  $z$  is the random variable. A particular instantiation of the exponential mechanism is the K-Norm Gradient mechanism [Reimherr and Awan, 2019, KNG]. KNG has been shown to have statistical utility gains in Euclidean spaces as compared to the exponential mechanism. This mechanism was extended to Riemannian manifolds by Soto et al. [2022] and shown to have similar utility gains as in the Euclidean case.

In general, the KNG mechanism on manifolds takes the form

$$f(z; D) \propto \exp\{-\sigma^{-1} \|\nabla E(z; D)\|_z\}. \quad (10)$$

KNG satisfies pure differential privacy when the noise scale is given by  $\sigma = \Delta/\epsilon$  where  $\Delta = \sup_{D \sim D'} \|\nabla E(z; D) - \nabla E(z; D')\|_z$  is the global sensitivity and  $\epsilon$  is the privacy budget or  $\sigma = 2\Delta/\epsilon$  if the normalizing constant is dependent on the footprint of the mechanism [Soto et al., 2022]. We further note that the sensitivity needs to be determined for ones choice of energy function.

### 3 Sensitivity bound using $k$ -norm mechanism

As discussed earlier we use the K-Norm Gradient (KNG) mechanism to sanitise the footprint and the shooting vector. For KNG to satisfy pure DP the sensitivity  $\Delta = \sup_{D \sim D'} \|\nabla E(z; D) - \nabla E(z; D')\|_z$  must be bounded. Since we estimate two parameters, each parameter has its own sensitivity bound. We let  $\Delta_p, \Delta_v$  be the sensitivity of the footprint and shooting vector, respectively. In this section we consider the sensitivity of the footprint  $\Delta_p$  and in D we consider the sensitivity of the shooting vector.

We wish to release a private version of  $p$  which is an optimizer of the energy function  $E(p, v; D)$  as in eqn 3. Since  $E(p, v; D)$  is a function of both  $p$  and  $v$  we must, in a sense, consider them separately as the gradient for KNG can be taken with respect to either parameter. For existence, uniqueness, and a finite sensitivity, we introduce the following assumptions.

**Assumption 3.1.** *The Riemannian manifold has sectional curvature bounded from above,  $\kappa_i \leq K_{max}$ .*

**Assumption 3.2.** *For dataset  $D \in \mathcal{D}$ , the data is bounded as  $D \subseteq B_r(m_0)$  where  $r \leq \frac{\pi}{8\sqrt{\kappa}}$  for symmetric spaces with positive curvature and  $r < \infty$  for symmetric spaces with negative curvature. Further the least-squares geodesic is  $\tau$ -close to the data with  $\tau > 0$ .*

**Lemma 3.3.** *Let Assumptions 3.1 and 3.2 hold. Let  $D, D'$  be adjacent datasets, for a fixed shooting vector  $v$ ,*

$$\begin{aligned} \Delta_p &= \sup_{D \sim D'} \|\nabla_p E(p; D) - \nabla_p E(p; D')\|, \\ &\leq \frac{2\tau}{n} \|J_p(1)\|, \end{aligned}$$

where  $J_p(1)$  is the Jacobi field.

*Proof.* Consider the sensitivity  $\sup_{D \sim D'} \|\nabla E(z; D) - \nabla E(z; D')\|_z$ . Take the shooting vector,  $v$ , as constant and focus on the footprint,  $p$ . The global sensitivity is

$$\Delta_p = \sup_{D \sim D'} \|\nabla_p E(p; D) - \nabla_p E(p; D')\|. \quad (11)$$

Fletcher [2011] showed that  $\nabla_p E(p; D) = -\frac{1}{n} \sum_{i=1}^n d_p \text{Exp}(p, x_i v)^\dagger \vec{\epsilon}_i$  where  $\vec{\epsilon}_i$  is the error vector and  $\dagger$  denotes the adjoint operator. The norm in eqn 11 is thus the difference of two sums that differ in only one term due to the adjacent datasets  $D \sim D'$ . All terms, thus, cancel except the last. We have,

$$\Delta_p = \frac{1}{n} \|d_p \text{Exp}(p, x_n v)^\dagger \epsilon_n \hat{e}_n - d_p \text{Exp}(p, x'_n v)^\dagger \epsilon'_n \hat{e}'_n\|, \quad (12)$$

$$= \frac{1}{n} \|d_p \text{Exp}(p, x_n v)^\dagger \epsilon_n \Gamma_{\epsilon_n}^p \hat{e}_n - d_p \text{Exp}(p, x'_n v)^\dagger \epsilon'_n \Gamma_{\epsilon'_n}^p \hat{e}'_n\|. \quad (13)$$

We use the convention that every vector can be written as a product of its magnitude and unit vector,  $\vec{q} = q \hat{q}$ . The adjoint operator  $\dagger$  can be thought of as an inner product on the tangent space after the required parallel transport. In the second line the operators  $\Gamma_{\epsilon_n}^p, \Gamma_{\epsilon'_n}^p$ , parallel transport  $\hat{e}'_n$  and  $\hat{e}_n$  to the tangent space of  $p$ .

By assumption  $\tau$  is the magnitude of the biggest possible error, the above expression maximizes when  $\epsilon_n = \epsilon'_n = \tau$  and  $\Gamma_{\epsilon_n}^p \hat{e}_n, \Gamma_{\epsilon'_n}^p \hat{e}'_n$  face in opposite directions. We get,

$$\Delta_p \leq \frac{1}{n} \|2\tau d_p \text{Exp}(p, x'_n v)^\dagger \Gamma_{\epsilon'_n}^p \hat{e}'_n\|, \quad (14)$$

$$\leq \frac{2\tau}{n} \|J_p(1)\|, \quad (15)$$

where  $J_p(1)$  is the Jacobi field with the initial conditions;  $J_p(0) = \Gamma_{\epsilon'_n}^p \epsilon'_n$ ,  $J'_p(0) = 0$ . Note that in the second to last line one could take either  $\epsilon'_n$  or  $\hat{\epsilon}_n$  but these produce the same bound under the assumption of  $\tau$ -closeness.  $\square$

The “sensitivity” in Lemma 3.3 is data-dependent because the Jacobi field’s initial conditions depend on data. The bound on sensitivity can be made global by using the Rauch theorem 2.1 as we show next.

**Theorem 3.4.** *If the manifold  $\mathcal{M}$  satisfies assumption 3.1 using Theorem 2.1 with  $\mathcal{M}$  as the manifold on which our data lies and  $\tilde{\mathcal{M}}$  as a manifold with constant sectional curvature  $K_{max}$ , then the tightest bound on the global sensitivity is given by:*

$$\Delta_p \leq \frac{2\tau}{n} \|\tilde{J}_p(1)\|, \quad (16)$$

where  $\|\tilde{J}_p(1)\|$  is the norm of the Jacobi field on a manifold with constant sectional curvature with initial conditions  $J_p(0) = \Gamma_u^p u$ ,  $u \in T_{\gamma(t)}\mathcal{M}$  for some  $t$ ,  $\|u\| = 1$ , and  $J'_p(0) = 0$ .

The sensitivity in Theorem 3.4 is the global sensitivity as the Jacobi field  $\tilde{J}_p$  has a closed-form solution that only depends on the upper bound on the sectional curvature  $K_{max}$  and the norm of the initial vector  $\Gamma_u^p u$  which is one.

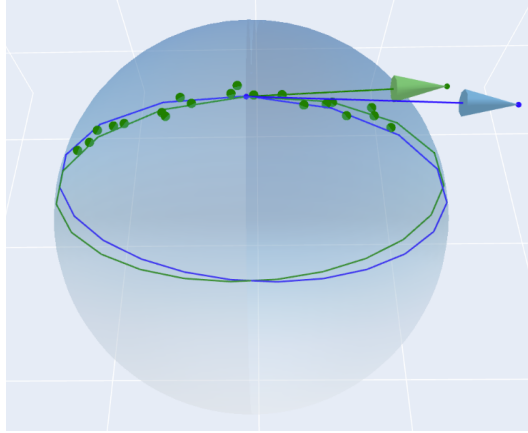


Figure 1: Twenty data points (green) on a unit sphere. The green curve is the geodesic formed with the pair  $(\hat{p}, \hat{v})$ . The blue curve is the private geodesic formed with the pair  $(\tilde{p}, \tilde{v})$ .

## 4 Experimental Results

### 4.1 Sphere

We create an artificial dataset of 20 datapoints on a unit sphere  $S_2$  by generating points on a geodesic and adding randomised errors to each point as shown in Figure 1. That is, we parametrise a geodesic by randomly picking a point  $q_0 \in S_2$  and a vector  $\zeta \in T_{q_0}\mathcal{M}$ . We then sample the geodesic  $\gamma(t) = \text{Exp}(q_0, t\zeta)$  uniformly on  $t \in [0, 1]$ , denote these as  $\{\gamma_i\}_{i=1, \dots, n}$ . These  $n$  points lie exactly on the geodesic. We add noise to the data points by sampling from a multivariate normal distribution with zero mean and a small covariance matrix  $(0.001 \times I_{3 \times 3})$ , ensuring independent perturbations in each dimension. Adding this noise, results in the data points lying outside the surface of the sphere therefore, we project the data points onto the unit sphere by normalization i.e.  $x \mapsto x/\|x\|$ . We note that  $q_0$  and  $\zeta$  need not be parameters of geodesic regression due to the randomness of the injected noise.

We denote the differentially private footpoint and shooting vector as  $\tilde{p}$  and  $\tilde{v}$  respectively. We aim to measure how the private estimates affect the energy  $E(p, v; D)$ . Using Riemannian Metropolis-Hastings as shown in appendix A, we first sample a set of DP footpoints  $(\tilde{p})$ , each with privacy budget

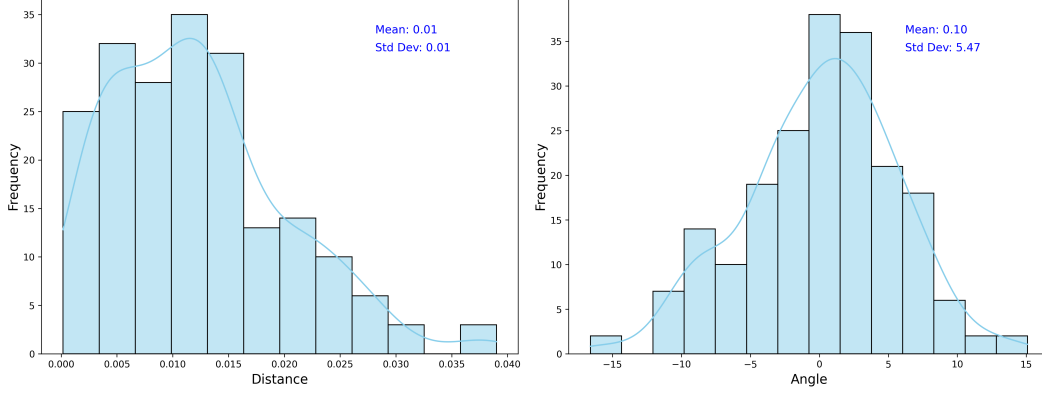


Figure 2: Histograms for 20 datapoints on a unit sphere of 200 samples. Left: Histogram of geodesic distance between  $\hat{p}$  and  $\tilde{p}_i \in \mathcal{P}$ . Right: Histogram of angles between  $\hat{v}$  and  $\tilde{v}_{1j} \in \mathcal{V}_1$ .

$\epsilon = 1$ , on the sphere denoted as  $\mathcal{P} = \{\tilde{p}_1, \tilde{p}_2, \dots, \tilde{p}_m\}$ . Since the energy is dependent on both a  $p$  and a  $v$ , for *each* footpoint we draw samples of many private shooting vectors. That is, on the tangent space of each footpoint  $\tilde{p}_i \in \mathcal{P}$ , we sample a corresponding set of private shooting vectors  $\mathcal{V}_i = \{\tilde{v}_{i1}, \tilde{v}_{i2}, \dots, \tilde{v}_{im}\}$ , each  $\tilde{v}$  sampled at a privacy budget of  $\epsilon = 1$ . Note that for each of the  $m$  many footpoints we sample  $m$  many shooting vectors on the respective tangent spaces yielding  $m^2$  many private pairs.

We form a differentially private geodesic curve with a footpoint  $\tilde{p}_i$  from the set  $\mathcal{P}$  and a shooting vector  $\tilde{v}_{ij}$  from the corresponding set  $\mathcal{V}_i$ . Each of these geodesics has a total privacy budget of  $\epsilon = 2$ , by composition. Let  $E_{ij} = \frac{1}{n} \sum_{k=1}^n d(\text{Exp}(p_i, x_k v_{ij}), y_k)$  be the Mean Absolute Error (MAE) between the data points  $\{y_k\}$  and the private predictions  $\{\tilde{y}_k\}$  from the DP geodesic formed by the selected  $\tilde{p}_i$  and  $\tilde{v}_{ij}$ . Next, let  $\mathcal{E}_i = \{E_{i1}, E_{i2}, \dots, E_{im}\}$  be the set of Mean Absolute Errors with a fixed footpoint  $p_i$  as the second index runs over the shooting vectors. Then  $\bar{\mathcal{E}}_i$  is the average of such a set. Recall that  $(\hat{p}, \hat{v})$  are the minimisers of the energy  $E(p, v; D)$ .

To evaluate the performance of our method we use three indicators: geodesic distances between  $\hat{p}$  and  $\tilde{p}_i \in \mathcal{P}$ ,  $d(\hat{p}, \tilde{p}_i)$ ; the angle between  $\Gamma_{\hat{p}}^{p_1} \hat{v}$  and  $\tilde{v}_{1j} \in \mathcal{V}_1$ ; and  $\bar{\mathcal{E}}_i$  for all footpoints  $p_i \in \mathcal{P}$  for  $i = 1, 2, \dots, m$ . That is, we measure deviations of the footpoint and shooting vector and the impact of privacy on the utility measured by the average energy.

The left panel of Figure 2 displays the distribution of geodesic distances between the 200 differentially private footpoint  $\tilde{p}_i$  and the true geodesic footpoint  $\hat{p}$ . The histogram demonstrates a narrow, right-skewed, concentrated distribution with a mean distance of 0.01 and standard deviation of 0.01. This indicates that the noise added to the footpoint by differential privacy is well-controlled and does not significantly distort the position of the geodesic footpoint. The relatively small distance values reflect the tight sensitivity bounds for the footpoint, confirming that our approach effectively balances privacy and accuracy in this component and the utility advantages of using a mechanism such as KNG.

The right panel of Figure 2 shows the angular deviation between the 200 differentially private shooting vector replicates  $\tilde{v}_{1j}$  and the true geodesic shooting vector  $\Gamma_{\hat{p}}^{p_1} \hat{v}$ . The true shooting vector is parallel transported to be on the tangent space of  $p_1$  as  $\Gamma_{\hat{p}}^{p_1} \hat{v}$ . The histogram shows a broader spread of angles with a mean of 0.10 degrees and a standard deviation of 5.47 degrees. While the noise added to the shooting vector results in more variation compared to the footpoint, the energy is not significantly impacted as shown later. Further, we note we expect the average angle to be about 0 as the shooting vector encodes direction. This is thus consistent with the expected higher sensitivity of the shooting vector.

Lastly, we also check the effect of privacy on the utility via the averages  $\bar{\mathcal{E}}_i$ ,  $i = 1, 2, \dots, m$ . The histogram in Figure 3 follows an unimodal distribution with a slightly right-skewed tendency, suggesting that the MAE values are concentrated near the lower end of the range but with a few instances of higher errors. The MAE found by using  $(\hat{p}, \hat{v})$  is 0.043 whereas the mean of the histogram is

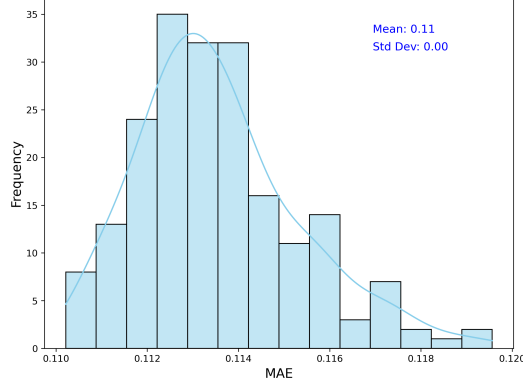


Figure 3: Histogram of  $\bar{\mathcal{E}}_i$ ,  $i = 1, 2, \dots, p$  for 20 datapoints on the sphere and 200 sampled replicates.

0.11 with standard deviation 0.00 (up to two decimal places). The small difference in the geodesic MAE and differentially private MAE and its low variability confirm the robustness of our approach to differentially private geodesic regression.

## 4.2 Euclidean Space

Using Theorem 3.4 and taking the Riemannian manifold as the Euclidean space we determine the sensitivities for differentially private geodesic regression. Our DP geodesic regression (DPGR) simplifies to a private linear regression in Euclidean space. For  $\mathbb{R}^n$  the norm of the Jacobi fields are  $\|J_p(1)\| = \|J_v(1)\| = 1$  resulting in the sensitivities  $\Delta_p = \Delta_v \leq \frac{2\tau}{n}$ .

We use the above sensitivities to compare our DPGR to IBM’s Diffprivlib [Holohan et al., 2019] and META’s Opacus [Yousefpour et al., 2022], which are two leading libraries for implementing differential privacy in machine learning. Diffprivlib, built in Python and compatible with scikit-learn, offers differentially private versions of classical models like linear regression. In contrast, Opacus is a PyTorch-based library focused on deep learning, using Differentially Private Stochastic Gradient Descent (DP-SGD), which combines gradient clipping to protect sensitive data.

Table 1: Comparison between differentially private linear regression models.

Model	Non-DP LR	<b>DPGR</b>	IBM DP	OPACUS DP
MSE	0.873	0.954	7.856	0.982

We assess the utility of our DPGR using artificially generated data, which is created by adding random errors to points on a line, as described in Subsection 4.1. Additionally, we use the Wine Quality dataset, restricting the analysis to the first 100 rows and selecting the following features: Fixed Acidity, Density, pH, and Residual Sugar.

Figure 4 presents the regression lines for four features of the wine quality dataset. The blue points represent the data, while the red line corresponds to the non-DP regression line, obtained using Scikit-learn’s Linear Regression model, which achieves a mean squared error (MSE) of 0.873. The blue line is plotted using regression parameters from our DPGR model achieving a MSE of 0.954. The green regression line represents the results from the IBM Diffprivlib package with a privacy budget of  $\epsilon = 2$ , aligning with our DPGR. The Diffprivlib regression line results in an MSE of 7.856, indicating that our DPGR outperforms IBM Diffprivlib by approximately 85 times.

Finally, the orange regression line is generated using the META Opacus package, also with a privacy budget of  $\epsilon = 2$ . The Opacus DP regression line results in an MSE of 0.982, demonstrating that our DPGR performs on par with the Opacus DP regression model. The MSE energies are mentioned in table 1.



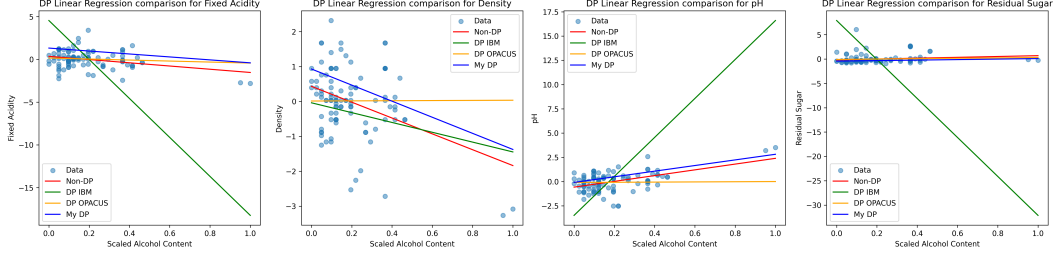


Figure 4: Comparison of differentially private (DP) and non-DP linear regression models for the Wine quality dataset. The blue scatter points are the original data points with regression lines from a non-private model (red) and three different DP methods: DP-IBM (green), DP-Opacus (orange), and our proposed DPGR (blue).

## 5 Discussion

Geodesic regression is an extension of linear regression to Riemannian manifolds. We have developed a methodology to release the parameters of geodesic regression (the footpoint and shooting vector) in a differentially private manner. To do so, we derive a theoretical bound on the sensitivity, under the KNG mechanism, of each parameter. We show that the sensitivity is a function of their respective Jacobi fields which itself is a function of the curvature of the manifold. A similar discovery was previously noted for the estimating the Fréchet mean by Reimherr et al. [2021], and Soto et al. [2022]. The authors note that positively curved manifolds, such as the  $n$ -sphere, inflate the sensitivity. We thus demonstrate our methodology on the 2-sphere, over a variety of sample sizes, as it is the more challenging case of curvature.

Interestingly, parametrising a geodesic poses an opportunity unique to manifolds. For instance, one can reverse the parametrisation of a geodesic  $\gamma : [0, 1] \rightarrow \mathcal{M}$  to  $\gamma^R : [1, 0] \rightarrow \mathcal{M}$ . One might consider such an endeavor if, for instance, the curvature of the manifold is *different* at the endpoints, i.e.  $\gamma(0)$  and  $\gamma(1)$ , thus directly affecting the sensitivity of  $\tilde{p}$ . Our methodology relies on an upper bound on the curvature but if more information is known, one can possibly leverage this information. We only considered the sphere which has constant positive curvature.

Similar to the standard exponential mechanism in Euclidean space, it is not straightforward to sample from KNG. This difficulty is compounded by the difficulty of sampling on manifolds. It would be interesting to develop an efficient sampler that utilizes the curvature of the manifold. Further, it would be particularly of interest to utilize this methodology on the positively curved Kendall’s shape space [Kendall, 1984], the complex projective space. This would be useful for computer vision where one can show regression of 2D shapes in a private manner. We emphasize that our methodology is fully compatible with private regression of shapes as this particular shape space is a Riemannian manifold.

## References

- D. Alabi, A. McMillan, J. Sarathy, A. Smith, and S. Vadhan. Differentially private simple linear regression. *arXiv preprint arXiv:2007.05157*, 2020.
- M. Bun and T. Steinke. Concentrated differential privacy: Simplifications, extensions, and lower bounds. In *Theory of cryptography conference*, pages 635–658. Springer, 2016.
- Y. Chen, Z. Lin, and H.-G. Müller. Wasserstein regression. *Journal of the American Statistical Association*, 118(542):869–882, 2023.
- M. P. Do Carmo. *Riemannian geometry*, volume 2. Springer, 1992.
- J. Dong, A. Roth, and W. J. Su. Gaussian differential privacy. *Journal of the Royal Statistical Society: Series B (Statistical Methodology)*, 84(1):3–37, 2022.
- C. Dwork and G. N. Rothblum. Concentrated differential privacy. *arXiv preprint arXiv:1603.01887*, 2016.
- C. Dwork, F. McSherry, K. Nissim, and A. Smith. Calibrating noise to sensitivity in private data analysis. In *Theory of cryptography conference*, pages 265–284. Springer, 2006.
- C. Dwork, K. Talwar, A. Thakurta, and L. Zhang. Analyze gauss: optimal bounds for privacy-preserving principal component analysis. In *Proceedings of the forty-sixth annual ACM symposium on Theory of computing*, pages 11–20, 2014.
- J. J. Faraway. Regression for non-euclidean data using distance matrices. *Journal of Applied Statistics*, 41(11):2342–2357, 2014.
- N. I. Fisher, T. Lewis, and B. J. Embleton. *Statistical analysis of spherical data*. Cambridge university press, 1993.
- P. T. Fletcher and S. Joshi. Principal geodesic analysis on symmetric spaces: Statistics of diffusion tensors. In *International Workshop on Mathematical Methods in Medical and Biomedical Image Analysis*, pages 87–98. Springer, 2004.
- T. Fletcher. Geodesic regression on riemannian manifolds. In *Proceedings of the Third International Workshop on Mathematical Foundations of Computational Anatomy-Geometrical and Statistical Methods for Modelling Biological Shape Variability*, pages 75–86, 2011.
- A. Han, P. Jawanpuria, and B. Mishra. Riemannian coordinate descent algorithms on matrix manifolds. *arXiv preprint arXiv:2406.02225*, 2024a.
- A. Han, B. Mishra, P. Jawanpuria, and J. Gao. Differentially private riemannian optimization. *Machine Learning*, 113(3):1133–1161, 2024b.
- N. Holohan, S. Braghin, P. M. Aonghusa, and K. Levacher. Diffprivlib: The ibm differential privacy library, 2019. URL <https://arxiv.org/abs/1907.02444>.
- J. Jeong, M. Jun, and M. G. Genton. Spherical process models for global spatial statistics. *Statistical science: a review journal of the Institute of Mathematical Statistics*, 32(4):501, 2017.
- Y. Jiang, X. Chang, Y. Liu, L. Ding, L. Kong, and B. Jiang. Gaussian differential privacy on riemannian manifolds. *Advances in Neural Information Processing Systems*, 36:14665–14684, 2023.
- D. G. Kendall. Shape manifolds, procrustean metrics, and complex projective spaces. *Bulletin of the London mathematical society*, 16(2):81–121, 1984.
- W. A. Link and M. J. Eaton. On thinning of chains in mcmc. *Methods in ecology and evolution*, 3(1): 112–115, 2012.
- F. McSherry and K. Talwar. Mechanism design via differential privacy. In *48th Annual IEEE Symposium on Foundations of Computer Science (FOCS’07)*, pages 94–103. IEEE, 2007.

- I. Mironov. Rényi differential privacy. In *2017 IEEE 30th computer security foundations symposium (CSF)*, pages 263–275. IEEE, 2017.
- M. Nakahara. *Geometry, topology and physics*. CRC press, 2018.
- A. Petersen and H.-G. Müller. Fréchet regression for random objects with euclidean predictors. *The Annals of Statistics*, 47(2):691–719, 2019.
- M. Reimherr and J. Awan. Kng: The k-norm gradient mechanism. *Advances in Neural Information Processing Systems*, 32, 2019.
- M. Reimherr, K. Bharath, and C. Soto. Differential privacy over riemannian manifolds. *Advances in Neural Information Processing Systems*, 34:12292–12303, 2021.
- O. Sheffet. Differentially private ordinary least squares. In *International Conference on Machine Learning*, pages 3105–3114. PMLR, 2017.
- O. Sheffet. Old techniques in differentially private linear regression. In *Algorithmic Learning Theory*, pages 789–827. PMLR, 2019.
- C. Soto, K. Bharath, M. Reimherr, and A. Slavković. Shape and structure preserving differential privacy. *Advances in Neural Information Processing Systems*, 35:24693–24705, 2022.
- Y.-X. Wang. Revisiting differentially private linear regression: optimal and adaptive prediction & estimation in unbounded domain. *arXiv preprint arXiv:1803.02596*, 2018.
- L. Wasserman and S. Zhou. A statistical framework for differential privacy. *Journal of the American Statistical Association*, 105(489):375–389, 2010.
- A. Yousefpour, I. Shilov, A. Sablayrolles, D. Testuggine, K. Prasad, M. Malek, J. Nguyen, S. Ghosh, A. Bharadwaj, J. Zhao, G. Cormode, and I. Mironov. Opacus: User-friendly differential privacy library in pytorch, 2022. URL <https://arxiv.org/abs/2109.12298>.

## A Sampling

This section describes how one could sample from the KNG mechanism on the unit sphere. We implement a Riemannian random walk Metropolis-Hastings algorithm to sample from the KNG mechanism. Suppose we have bounds on the sensitivity of  $p$  and  $v$ , denoted  $\Delta_p$  and  $\Delta_v$  respectively, as in 3.

We have that  $f(p; D) \propto \exp\{-\sigma^{-1}\|\nabla_p E(p; D)\|_p\}$ . Given that  $\sigma = \Delta_p/\epsilon$  and the gradient is as in 3,

$$\begin{aligned} f(p; D) &\propto \exp\left\{-\frac{\|\nabla_p E(p; D)\|_p}{\Delta_p/\epsilon}\right\} \\ &= \exp\left\{-\frac{\| -1/n \sum d^2(\text{Exp}(p, x_i v), y_i) \|_p}{2\tau \|J_p(1)\|/n}\right\} \\ &= \exp\left\{-\frac{\|\sum d^2(\text{Exp}(p, x_i v), y_i) \|_p}{2\tau \|J_p(1)\|}\right\}. \end{aligned}$$

For a Riemannian manifold such as a unit sphere with curvature  $K = 1$ , we can solve eqn 1 to find the norm of the Jacobi field  $\|J_p(1)\|$ . We have

$$\frac{D^2}{dt^2} J_p(t) + J_p(t) = 0, \quad (17)$$

remembering that the initial conditions are  $J_p(0) = \Gamma_{\epsilon_n}^{\epsilon_n'} \hat{\epsilon}_n'$ ,  $J'(0) = 0$  we get:

$$\|J_p(1)\| = \cos(1). \quad (18)$$

Similarly the initial conditions for  $J_v(t)$  are  $J_v(0) = 0$ ,  $J'_v(0) = \Gamma_{\epsilon_n}^{\epsilon_n'} \hat{\epsilon}_n$  giving us,

$$\|J_v(1)\| = \sin(1). \quad (19)$$

To sample from this distribution, first, initialize the random walk at  $p_0$  which can be any data point, the Fréchet mean of the points, or the sample statistic  $\hat{p}$ . To make a proposal we first sample a vector  $\nu_{prop}$  from the tangent space, as it is simply a Euclidean plane, uniformly around  $p_0$  with a radius  $\eta$ . This  $\eta$  is a tuning parameter that determines the ‘stickiness’ of the MCMC chain. We set  $\eta \propto \sigma$ . The proposal is then  $p_{prop} = \text{Exp}(p, \nu_{prop})$ . Typically one would then compute the acceptance probability, however, note that the energy depends on both the shooting vector *and* a footprint. Since we are under the assumption  $v$  is constant, we parallel transport  $v$  to the proposal that is, we use  $\Gamma_{\hat{p}}^{p_{prop}} \hat{v}$ . Lastly, compute the acceptance probability in the typical fashion  $f(p_{prop}; D)/f(p_0; D)$ . We draw subsequent instances in the same fashion continuing the random walk from the previously accepted footprint. We forego thinning the chain as it has been argued that it is not a necessary procedure [Link and Eaton, 2012]. Furthermore, thinning decreases efficiency which compounds with the inefficiency of sampling on manifolds. While sampling instead of  $\tau$  we use  $\max \|\epsilon_i\|$ , the empirical largest error, in the acceptance probability as the largest error in the dataset.

## B Validity of sensitivity bounds

In this section, we present evidence of the validity of the sensitivity bounds found in Section 3. We create artificial adjacent datasets  $D, D'$  each of  $n$  data points on a unit sphere. This is done by generating  $n + 1$  data points on the sphere by the same mechanism mentioned at the start of Section 4 and removing the first data point for the dataset  $D$  and the last data point for the dataset  $D'$ .

Let us define an experimental sensitivity for the footprint  $p$  as  $\Delta_p^{exp} = \|\nabla_p E(p; D) - \nabla_p E(p; D')\|$  and for the shooting vector  $v$  as  $\Delta_v^{exp} = \|\nabla_v E(p; D) - \nabla_v E(p; D')\|$ . We call these experimental bounds as the gradients depend on the generated datasets. Next, we define theoretical sensitivity bounds as,  $\Delta_p^{thy} = \sup_{D \sim D'} \|\nabla_p E(p; D) - \nabla_p E(p; D')\|$  and  $\Delta_v = \sup_{D \sim D'} \|\nabla_v E(v; D) - \nabla_v E(v; D')\|$ . From section 3 we know that the theoretical bounds are given by  $\Delta_p^{thy} = \frac{2\tau}{n} \|J_p(1)\|$  and  $\Delta_v^{thy} = \frac{2\tau}{n} \|J_v(1)\|$ . Here we take  $\tau = \max_{D, D'} \{\epsilon_j\}$ , where  $\{\epsilon_j\}$  is the combined set of errors in datasets  $D, D'$ . To check the validity of our theoretical sensitivity bounds we calculate the ratios

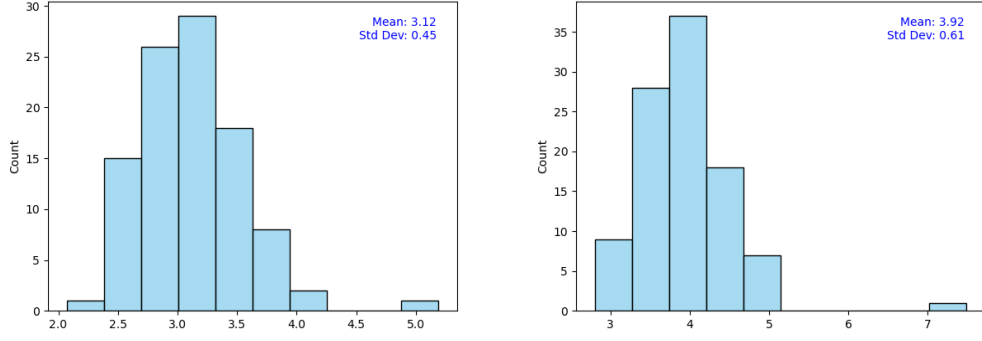


Figure 5: Each histogram is generated with 100 pairs of adjacent datasets each with 20 data points on a unit sphere. Left: Histogram of the ratio  $r_p = \Delta_p^{thy} / \Delta_p^{exp}$ . Right: Histogram of the ratio  $r_v = \Delta_v^{thy} / \Delta_v^{exp}$ .

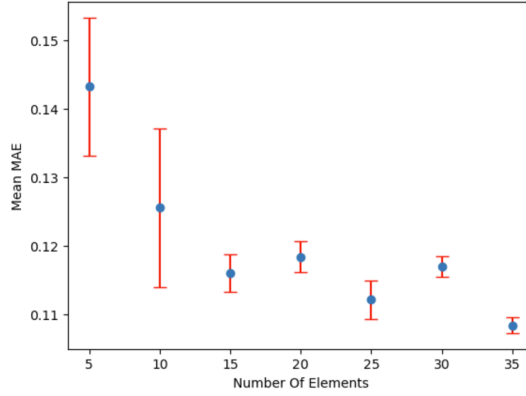


Figure 6: Mean of the histogram of  $\bar{\mathcal{E}}_i$ ,  $i = 1, 2, \dots, p$  versus number of elements on the unit sphere for 11 sampled  $\tilde{p}, \tilde{v}$  replicates. The error bars (red) indicate the standard deviation, which decreases as we increase the number of elements.

$r_p = \frac{\Delta_p^{thy}}{\Delta_p^{exp}}, r_v = \frac{\Delta_v^{thy}}{\Delta_v^{exp}}$ . We expect the theoretical bounds to be always greater than the experimental ones as they are defined to be the supremum over all possible adjacent datasets. Thus the ratios  $r_p$  and  $r_v$  are expected to be greater than one.

To check the validity of our sensitivity bounds we generate adjacent datasets with  $n = 20$  datapoints on the sphere as described earlier. Figure 5 shows the histograms for the ratios  $r_p, r_v$  for 100 such pairs of adjacent datasets. Values closer to one demonstrate the tightness of the bound and no values being smaller than one demonstrate the validity. As can be seen in both panels of Figure 5 ratios  $r_p, r_v$  are always greater than one. Both the histograms are right-skewed with the mean of the histogram for  $r_p$  being 3.12 and the mean for  $r_v$  is 3.92. This shows that our theoretical bounds are tight and gives compelling evidence for the validity of the sensitivity bounds.

Additionally, we have checked how the mean of the histogram in Figure 3 changes with the number of elements,  $n$ , on the unit sphere. As we increase the number of elements on the sphere, the acceptance probability decreases and the sampled  $(\tilde{p}, \tilde{v})$  are very close to the geodesic  $(\hat{p}, \hat{v})$ . This results in the mean MAE non-linearly converging to the geodesic energy as seen in Figure 6. The reduction in variability, as reflected by the smaller error bars for a larger number of elements, further supports the method's robustness. We note that we have considered 11 sampled replicates for  $(\tilde{p}, \tilde{v})$  as sampling requires a significantly extended computational duration as the number of elements increases.

## C Riemannian Geometry

Following Nakahara [2018] we elaborate on two important aspects of Riemannian geometry that are widely used in this paper.

### C.1 Parallel transport

On a Riemannian manifold, the metric  $g$  induces a natural volume form with the help of a local basis  $\{\partial/\partial x^i\}$  given by  $\text{vol}_g = \sqrt{\det g} dx^1 \wedge dx^2 \cdots \wedge dx^n$ . The Riemannian measure  $d\mu_g$  is derived using the volume form and allows us to integrate over the manifold,

$$d\mu_g = \sqrt{\det g} dx^1 dx^2 \cdots dx^n.$$

Any subset of the manifold  $A \subset \mathcal{M}$  is measurable if it belongs to the  $\sigma$ -algebra  $\mathcal{M}$  associated with the Riemannian measure.

The generalization of a Euclidean shortest path, straight lines, on Riemannian manifolds is referred to as a “geodesic.” A connection  $\nabla$  on a manifold can be used to take directional derivatives and thus define a geodesic curve. A curve  $\gamma : [0, 1] \rightarrow \mathcal{M}$  on  $\mathcal{M}$  is a geodesic curve with respect to  $\nabla$  if its acceleration is zero i.e.  $\nabla \dot{\gamma} = 0$ . On a manifold with linear connection there always exists a unique geodesic which is denoted by a footpoint  $p$  and shooting vector  $v \in T_p \mathcal{M}$ . The distance,  $d(\cdot, \cdot)$ , between two points  $p, q \in \mathcal{M}$  is thus the length of the geodesic between them  $d(p, q) := \mathcal{L}(\gamma) = \int \|\dot{\gamma}(t)\|_{\gamma(t)}^{1/2} dt$ .

Parallel transport plays a crucial role in proving theorem 3.3 and sampling replicates for the MCMC chain. Unlike Euclidean space comparing two vectors on a general manifold  $\mathcal{M}$  becomes more challenging as the vector can lie on different tangent spaces of  $\mathcal{M}$ . Consider two points on the manifold close to each other,  $x, x + \delta x$ . We can have a vector field on the tangent space of  $x$  given by  $V = V^\mu e_\mu$  where  $e_\mu$  is the local basis and  $V_\mu$  are the vector components. In Euclidean space the derivative with respect to  $x^\nu$  is given by:

$$\frac{\partial V^\mu}{\partial x^\nu} = \lim_{\delta x \rightarrow 0} \frac{V^\mu(\cdots, x^\nu + \delta x^\nu, \cdots) - V^\mu(\cdots, x^\nu, \cdots)}{\delta x^\nu} \quad (20)$$

On a general manifold, we need to transport  $V^\mu(x)$  to  $x + \delta x$  to perform the above subtraction. Denote a vector  $V(x)$  transported to  $x + \delta x$  as  $\tilde{V}(x + \delta x)$  and satisfies the following conditions,

$$\tilde{V}^\mu(x + \delta x) - V^\mu(x) \propto \delta x \quad (21)$$

$$\widetilde{V^\mu + W^\mu} = \tilde{V}^\mu(x + \delta x) + W^\mu(x + \delta x). \quad (22)$$

A transport is called *parallel transport* if the above conditions are satisfied. There are distinct rules of parallel transport and one can write them in short by using a *connection*. The above definition of parallel transport can be written as  $\Gamma \tilde{V}^\mu(x + \delta x) = V^\mu(x) - V^\lambda(x) \Gamma_{\nu\lambda}^\mu \delta x^\nu$ . For a manifold with a metric, there is a preferred choice of  $\Gamma$  called as Levi-Civita connection to define the parallel transport. Using the connection we can thus define a covariant derivative which is similar to a directional derivative in Euclidean space as,

$$\nabla_\mu V^\lambda = \frac{\partial V^\lambda}{\partial x^\mu} + \Gamma_{\mu\nu}^\lambda W^\nu, \quad (23)$$

where  $\nabla_\mu W^\lambda$  is the  $\lambda$ th component of a vector  $\nabla_\mu W$ .

### C.2 Riemannian curvature tensor

The geometric meaning of the curvature of a manifold and the Riemann curvature tensor is understood by parallel transporting a vector  $V_0$  at  $p$  to a different point  $q$  along two distinct curves  $C$  and  $C'$ . One can notice in Figure 7 that the resulting two vectors are different from each other. This non-integrability of parallel transport defines the intrinsic notion of curvature of a manifold.

Take four points on a manifold defined by the vertices of an infinitesimal parallelogram,  $p \equiv x^\mu, q \equiv x^\mu + \epsilon^\mu, s \equiv x^\mu + \delta^\mu, r \equiv x^\mu + \delta^\mu + \epsilon^\mu$ . We can parallel transport a vector  $V_0$  along two curves

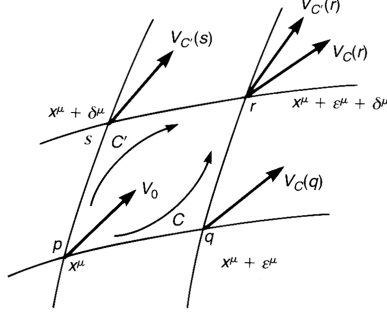


Figure 7: The vector  $V_0$  is parallel transported along the curves  $C$  and  $C'$  resulting in  $V_C(r)$  and  $V_{C'}(r)$ . The difference between these resulting vectors at the point  $r$  represents the curvature of the manifold Nakahara [2018].

defined by  $C = p q r$  and  $C' = p s r$ . The resulting vectors  $V_C^\mu(r)$  and  $V_{C'}^\mu(r)$  can be written in terms of the original vector  $V_0 \in T_p \mathcal{M}$  as,

$$V_C^\mu(r) = V_0^\mu - V_0^\kappa \Gamma_{\nu\kappa}^\mu(p) \epsilon^\nu - V_0^\kappa \Gamma_{\nu\kappa}^\mu(p) \delta^\nu - V_0^\kappa (\partial_\lambda \Gamma_{\nu\kappa}^\mu(p) - \Gamma_{\lambda\kappa}^\rho(p) \Gamma_{\nu\rho}^\mu(p)) \epsilon^\lambda \delta^\nu \quad (24)$$

$$V_{C'}^\mu(r) = V_0^\mu - V_0^\kappa \Gamma_{\nu\kappa}^\mu(p) \delta^\nu - V_0^\kappa \Gamma_{\nu\kappa}^\mu(p) \epsilon^\nu - V_0^\kappa (\partial_\nu \Gamma_{\lambda\kappa}^\mu(p) - \Gamma_{\nu\kappa}^\rho(p) \Gamma_{\lambda\rho}^\mu(p)) \epsilon^\lambda \delta^\nu. \quad (25)$$

Once we have parallel transported the vectors on the tangent space of  $r$  we can quantify their difference as

$$V_{C'}^\mu(r) - V_C^\mu(r) = V_0^\kappa (\partial_\lambda \Gamma_{\nu\kappa}^\mu(p) - \partial_\nu \Gamma_{\lambda\kappa}^\mu(p) - \Gamma_{\lambda\kappa}^\rho(p) \Gamma_{\nu\rho}^\mu(p) + \Gamma_{\nu\kappa}^\rho(p) \Gamma_{\lambda\rho}^\mu(p)) \epsilon^\lambda \delta^\nu \quad (26)$$

$$= V_0^\kappa R_{\kappa\lambda\nu}^\mu \epsilon^\lambda \delta^\nu. \quad (27)$$

The Riemann curvature tensor ( $R_{\kappa\lambda\nu}^\mu$ ) is defined as this difference and represents the curvature.

## D Sensitivity bound for the shooting vector

In section 3 it was shown how to bound the sensitivity for the footprint. In this section, we give the theorem with proof to bound the sensitivity for the shooting vector. As before we will use the KNG mechanism focusing on the shooting vector. If the assumption 3.1 and 3.2 are satisfied the bound on the sensitivity  $\Delta_v$  is given by:

**Theorem D.1.** *Let Assumptions 3.1 and 3.2 hold. Let  $D, D'$  be adjacent datasets, for a fixed footprint  $p$ ,*

$$\begin{aligned} \Delta_v &= \sup_{D \sim D'} \|\nabla_v E(v; D) - \nabla_v E(v; D')\| \\ &\leq \frac{2\tau}{n} \|J_v(1)\|, \end{aligned}$$

where  $J_v(1)$  is the Jacobi field and  $\epsilon_m \geq 0$  is a bound on the norm of the residuals.

*Proof.* Consider the sensitivity  $\sup_{D, D'} \|\nabla E(z; D) - \nabla E(z; D')\|_z$ . We will take the footprint  $p$ , as constant. The global sensitivity is

$$\Delta_v = \sup_{D \sim D'} \|\nabla_v E(v; D) - \nabla_v E(v; D')\|. \quad (28)$$

We have that  $\nabla_v E(v; D) = -\frac{1}{n} \sum_{i=1}^n x_i d_v \text{Exp}(p, x_i v)^\dagger \vec{\epsilon}_i$  where  $\vec{\epsilon}_i$  is the error vector and  $\dagger$  denotes the adjoint operator. The norm in eqn 28 is the difference of two sums that differ in only one term due to the adjacent datasets  $D \sim D'$ . All terms thus cancel except the last. Here,  $x_n, x'_n$  as elements of  $D, D'$ , respectively. Thus,

$$\Delta_v = \frac{1}{n} \|x_n d_v \text{Exp}(p, x_n v)^\dagger \epsilon_n \hat{\epsilon}_n - x'_n d_v \text{Exp}(p, x'_n v)^\dagger \epsilon'_n \hat{\epsilon}'_n\| \quad (29)$$

$$= \frac{1}{n} \|x_n d_v \text{Exp}(p, x_n v)^\dagger \epsilon_n \Gamma_{\epsilon_n}^p \hat{\epsilon}_n - x'_n d_v \text{Exp}(p, x'_n v)^\dagger \epsilon'_n \Gamma_{\epsilon'_n}^p \hat{\epsilon}'_n\|. \quad (30)$$

Remember that the adjoint operator  $\dagger$  can be thought of as an inner product on the same tangent space after the required parallel transport. In the second line the operators  $\Gamma_{\epsilon_n}^p, \Gamma_{\epsilon'_n}^p$  parallel transports  $\epsilon_n$  and  $\epsilon'_n$  to the tangent space of  $p$ .

Let  $\tau$  be the magnitude of largest possible error, the above expression maximizes when  $x_n = x'_n = 1$  and  $\epsilon'_n = \epsilon_n = \tau$  with  $\Gamma_{\epsilon'_n}^p \hat{\epsilon}_n', \Gamma_{\epsilon_n}^p \hat{\epsilon}_n$  face in opposite directions. We get,

$$\Delta_v \leq \frac{1}{n} \|2 \tau d_v \text{Exp}(p, x_n v)^\dagger \Gamma_{\epsilon_n}^p \hat{\epsilon}_n\| \quad (31)$$

$$\leq \frac{2 \tau}{n} \|J_v(1)\|, \quad (32)$$

where  $J_v(1)$  is the Jacobi field with  $J_v(0) = 0, J'_v(0) = \Gamma_{\epsilon_n}^p \hat{\epsilon}_n$ . This completes the proof.  $\square$

One can notice that the Jacobi field in the above bound is data depended due to the initial conditions. As before we can find the global sensitivity when assumption 3.1 is satisfied by using theorem 2.1.

$$\Delta_v \leq \frac{2 \tau}{n} \|\tilde{J}_v(1)\|. \quad (33)$$

The Jacobi field  $\tilde{J}_p$  has a closed-form solution that depends on the sectional curvature  $K_{max}$  making the sensitivity not data dependent.